Synthesis and Electrochemical Behavior of Crystalline Ag_2Se Nanotubes

Sheng-Yi Zhang,*,† Chun-Xia Fang,† Wei Wei,† Bao-Kang Jin,† Yu-Peng Tian,† Yu-Hua Shen,† Jia-Xiang Yang,† and Hong-Wen Gao‡

Department of Chemistry, Anhui University, Hefei 230039, China, and College of Environmental Science and Engineering, Tongji University, Shanghai 200092, China

Received: November 9, 2006; In Final Form: January 12, 2007

A novel chemical method has been developed for the preparation of crystalline nanotubes of silver selenide (Ag_2Se). The method is based on the template-engaged synthesis in which the trigonal Se nanotubes as-prepared were used as template reagent. The products were characterized by scanning electron microscopy (SEM), X-ray diffraction (XRD), energy-dispersive X-ray analysis (EDX), transmission electron microscopy (TEM), ultraviolet (UV) analysis, photoluminescence (PL) analysis, differential scanning calorimetric (DSC) analysis, and thermogravimetric (TG) analysis. Based on a series of experiments and characterizations, the formation mechanism of the Ag_2Se nanotubes was proposed. Furthermore, the useful electrochemical behavior of the Ag_2Se nanotubes was studied by the voltammetric technique.

Introduction

In past decades, silver selenide (Ag_2Se) has received great attention due to its interesting and useful characteristics.[1−6] Ag_2Se can exist as a low-temperature phase (α-Ag_2Se) and a high-temperature phase (β-Ag_2Se).[7] The α-Ag_2Se, as an n-type semiconductor with a narrow band gap, is useful as a photosensitizer and a thermoelectric material,[8] whereas the β-Ag_2Se is a superionic conductor that can be used as the solid electrolyte in photochargable secondary batteries.[9] In addition, large positive and negative magnetoresistance effects have been found for the nonstoichiometric derivative of Ag_2Se.[5] Therefore, it is reasonable to expect that the unique structure and property of Ag_2Se nanostructures would introduce new applications or enhance the performance of the existing devices. A number of methods for the synthesis of Ag_2Se nanostructures have been explored, such as vacuum evaporation,[10] flash evaporation,[11] sequential evaporation,[12] chemical bath deposition,[13] solvothermal reaction,[14] sonochemical reaction,[15] and the conversion of Ag nanoparticles[16] or Se nanoparticles.[17] However, most objects of these syntheses are the films or spherical particles of Ag_2Se.

As is well-known, the solid template synthesis in which the template served as a physical scaffold has been extensively applied to prepare one-dimensional (1D) nanostructures. In some cases, the template could act as one of the reactants and engage in the synthesis process. On the basis of this template-engaged synthesis, Byron et al. prepared the Ag_2Se nanowires that were formed by templating against Se or Ag nanowires.[9,18] Jiang et al. converted Se nanowires to Se/Ag_2Se nanocables that were further transformed to Ag_2Se nanotubes through irradiating the nanocables by the electron beams.[19] Bernard et al. synthesized Ag_2Se nanotubes by UV photodissociation of adsorbed CSe_2 on the surface of Ag nanowires.[20] In this paper, we describe a template-engaged synthesis for single-crystalline Ag_2Se nanotubes, in which the single-crystalline nanotubes of trigonal Se (t-Se) as-prepared were used as template reagent. The advantage of the present method is that the synthesis could be rapidly carried out in aqueous media, and the morphology of the Ag_2Se nanotubes could be controlled because the reaction scope was confined by the Se nanotubes. Based on a series of experiments and characterizations, the effect factors on synthesis and the formation mechanism of the Ag_2Se nanotubes were discussed. In addition, the electrochemical behavior of the Ag_2Se nanotubes was studied by voltammetric technique, and the results obtained would help to understand Ag_2Se's interband properties, which are significant in a variety of diverse fields.

Experimental Section

Synthesis. All of the reagents are of analytical grade and were used in experiments without further purification. The t-Se nanotubes to be used as template reagent for the synthesis of Ag_2Se nanotubes were synthesized as described in our report.[21] Typically, the synthesis experiment for Ag_2Se nanotubes was carried out as follows. First, 0.1 mmol of t-Se nanotubes was added into aqueous $AgNO_3$ (0.3 mmol) solution under stirring. Next, the mixture solution was kept still in a water bath for 1 h at 60 °C. Finally, the fuscous product formed in the solution was separated out by centrifuging and washed several times with hot water (90 °C).

Characterization. The product as-obtained was characterized by scanning electron microscopy (SEM), energy-dispersive X-ray analysis (EDX, 1530 VP Ger. LEO with OXFORD INCA-300), transmission electron microscopy (TEM, TEOL JEM-100SX), X-ray diffraction (XRD, Japan Rigaku D/max-RA X-ray diffractometer, with graphite monochromatized Cu $K\alpha_1$ radiation, $\lambda = 0.15406$ nm), ultraviolet absorption (UV-3600, Japan), and photoluminescence analysis (PL, F-2500, Japan). The thermogravimetric (TG) analysis and differential scanning calorimetric (DSC) analysis were carried out on a TG/DSC apparatus (Pyris-1, Perking Elmer, USA, at a heating rate of 20 °C/min in a flowing high-purity nitrogen gas with 20 mL/min).

Electrochemistry. The electrochemical behavior of the product was studied by potential scan voltammetry on an electrochemical system (MPI-A, Xi'an, China). The electro-

* Corresponding author. Tel/fax: +86 551 5107342. E-mail: syzhangi@126.com.
† Anhui University.
‡ Tongji University.

10.1021/jp067425d CCC: $37.00
Published on Web 03/01/2007

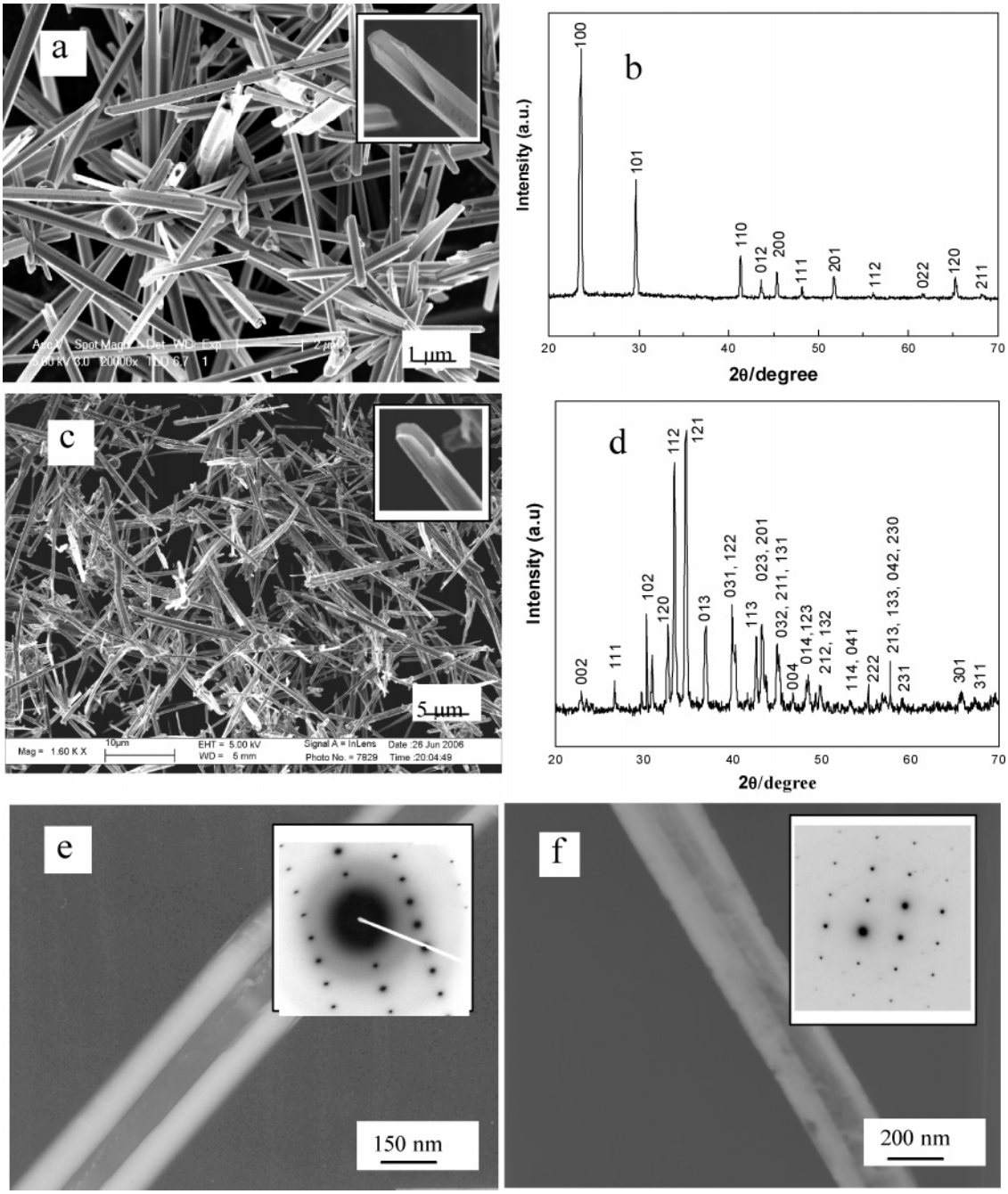

Figure 1. (a) SEM image of Se product (the inset shows the mouth of a nanotube); (b) XRD pattern of Se product; (c) SEM image of Ag_2Se product (the inset shows the mouth of a nanotube); (d) XRD pattern of Ag_2Se product; (e) TEM image of Se product (the inset shows a typical microdiffraction pattern); and (f) TEM image of Ag_2Se product (the inset shows a typical microdiffraction pattern).

chemical cell was made up of a given electrolyte solution and a three-electrode system: a platinum sheet counter electrode, an Ag/AgCl/1 M KCl/1 M KNO_3 double junction reference electrode against which all potentials were recorded, and a working carbon paste electrode that was prepared as follows. First, the carbon paste was prepared by paraffin binding the mixture of graphite powder (100 mg) and Ag_2Se product (10 mg). Next, the carbon paste electrode (CPE) was obtained by filling the carbon paste into a port of the glass tube (Φ 3 mm) that was linked with a copper wire. Prior to experiment, the surface of CPE was polished with fine paper and the electrolyte solution was degassed with N_2. The potential scan rate was 10 mV/s for all electrochemical experiments, except the situation specialized.

Caution! The Se-containing solutions are toxic; thus adequate care is demanded in the handling and disposal of these solutions.

Results and Discussion

Characterization. The tubular morphology of the Se product to be used as the template for the synthesis of Ag_2Se was disclosed by SEM (Figure 1a). The wide-angle XRD result (Figure 1b) indicates that the Se nanotubes are made up of the trigonal phase Se (t-Se) (JCPDS Card, No. 6-362). The SEM image (Figure 1c) shows the tubular morphology of the Ag_2Se product obtained in typical condition. In addition, from the SEM image, it can be seen that the Ag_2Se product maintains closely the morphology of the initial t-Se templates. The crystallization of the Ag_2Se product was confirmed by wide-angle XRD. The diffraction peaks in the XRD pattern (Figure 1d) can readily be indexed to the orthorhombic phase (β-Ag_2Se), and no impurity diffraction peaks were detected, such as Se, Ag, or Ag_2O peaks.

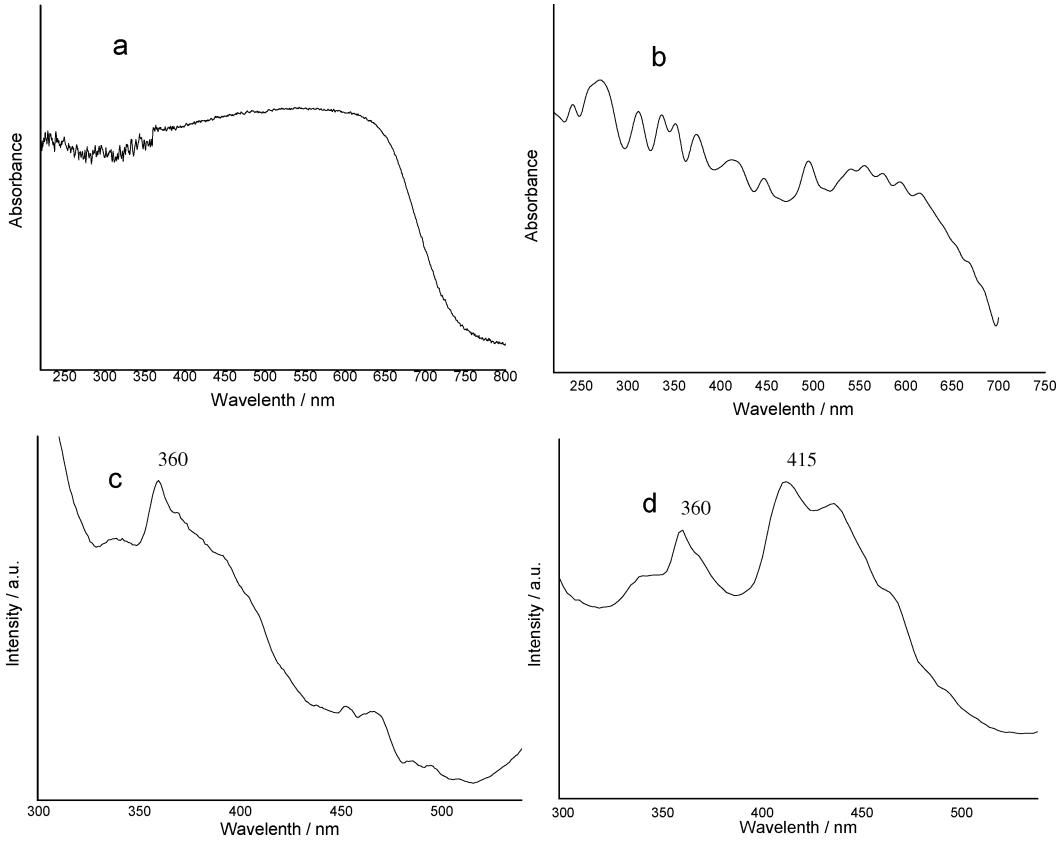

Figure 2. UV−vis absorption patterns of Se nanotubes (a) and Ag_2Se nanotubes (b); PL emission patterns (with 280 nm excitation) of Se nanotubes (c) and Ag_2Se nanotubes (d).

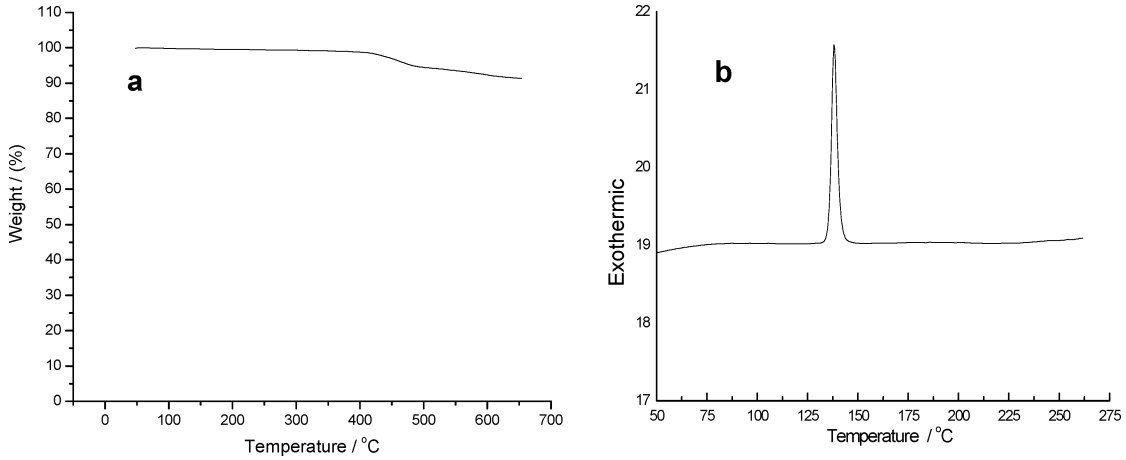

Figure 3. The patterns recorded from a bulk quantity of the Ag_2Se nanotubes: (a) the TG curve; and (b) the DSC curve.

The unit cell constants calculated from this diffraction pattern are $a = 0.4336$ nm, $b = 0.7053$ nm, and $c = 0.7781$ nm, which agree well with the literature data for β-Ag_2Se (JCPDS Card, No. 24-1041). The result of the EDX shows that the atom ratio of the Ag and Se in this tubular product is 65.63:34.37, close to the stiochiometric composition of the Ag_2Se. The tubular characteristics of the Se and Ag_2Se products as-synthesized were further confirmed by TEM images (Figure 1e and f). From Figure 1f, it can be seen that the typical Ag_2Se nanotube is 50 nm in thickness of wall and 200 nm in diameter. The electron diffraction pattern (ED, as inset in TEM image) obtained by focusing the electron beam on an individual nanotube confirms that the nanotubes are single crystalline.

Typical UV−vis absorption spectra of the products are shown in Figure 2a and b. From the spectra, it can be seen that the UV−vis absorption edge of Ag_2Se nanotubes has a small blue shift relative to that of Se nanotubes. According to the relationship of the band gap energy (E_g) with the absorption edge, the E_g of the Ag_2Se nanotubes was calculated to be 1.77 eV that agrees well with the value reported.[13] The results of the room-temperature PL analysis are shown in Figure 2c and d. The PL peak at 360 nm (Figure 2c) of Se nanotubes is similar to that of Se nanowires as reported.[22] On the PL spectrum (Figure 2d) of Ag_2Se nanotubes, there is a strong PL peak at 415 nm that may result from the direct interband radiative recombination.[22] The weak PL peak at 360 nm (Figure 2d) may come from the remainder elemental Se in Ag_2Se product.

The result of thermal analysis for the Ag_2Se product is shown in Figure 3. From the TG curve (Figure 3a), it is obvious that the mass of the sample remains nearly constant in the range of 100−400 °C, and then the mass decreases slightly on heating over 450 °C. This mass decrease may be relative to the

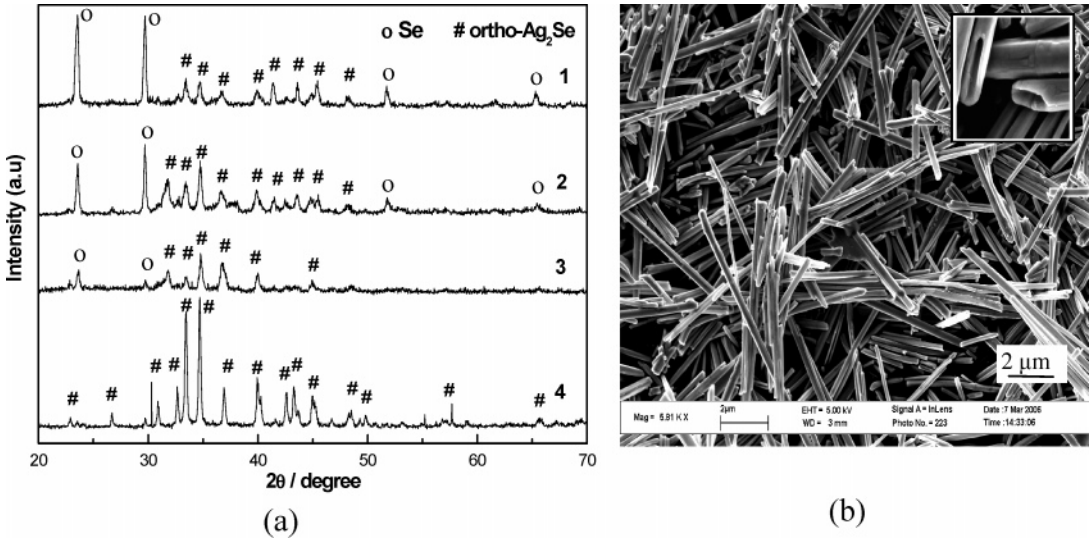

Figure 4. (a) The XRD patterns of the products obtained with different reaction times at room temperature: (1) 1 h; (2) 1 d; (3) 7 d; (4) 10 d. (b) The SEM image of the product obtained in 7 d (the upper inset shows the mouth of nanotubes).

sublimation of little remainder elemental Se in Ag_2Se product. From the DSC curve (Figure 3b), it can be seen that a symmetric endothermic peak exhibits at 138 °C, which can be assigned to the melting point of the sample because the sample has no loss or gain of mass at this temperature (as shown in Figure 3a). According to the literature,[15] this endothermic reaction corresponds to the transition from the orthorhombic phase (β-Ag_2Se) to the tetragonal phase (α-Ag_2Se). Besides, the symmetry of the endothermic peak suggests the phase homogeneity of the product as-prepared.[4]

Formation Process. Consulting the literature,[9,18] the formation process of Ag_2Se nanotubes is proposed as follows. First, the Ag^{1+} (in $AgNO_3$ aqueous solution) diffused into the crystal lattice of t-Se nanotubes and catalyzed the disproportion of Se^0 (in Se nanotubes) to Se^{2-} and Se^{4+}. Next, the Se^{2-} species was produced, combined with the Ag^{1+} to form Ag_2Se crystal within the solid matrix (Se nanotubes), whereas Se^{4+} species synchronously produced, diffused out of the solid matrix, and were transformed to Ag_2SeO_3 by reacting with H_2O and Ag^{1+}. The reaction equation is expressed as:

$$3Se\,(s) + 6Ag^{+}\,(aq) + 3H_2O\,(aq) \rightarrow 2Ag_2Se\,(s) + Ag_2SeO_3\,(s) + 6H^{+}\,(aq)$$

Similar to the formation mechanism of the Ag_2Se nanowires by templating against t-Se nanowires,[18] the Ag_2Se nanotubes were finally produced through the topotactic transformation of t-Se nanotubes. It is worthy pointing out that the solid byproduct Ag_2SeO_3 formed in out of the solid matrix can be easily removed by washing the product with hot water (90 °C).

It has been found that the system temperature markedly affected the formation speed of Ag_2Se nanotubes. As above, the transition from t-Se nanotubes to Ag_2Se nanotubes was achieved in 1 h at 60 °C. When the temperature was increased to 80 °C, this transition was completed in a shorter period of time (30 min). Contrarily, the speed of the transition was largely slowed at low temperature. Figure 4a shows the XRD patterns of the products obtained at various room-temperature (RT) reaction stages. The assignment of the diffraction peaks gives a clear insight into the transition degree of t-Se nanotubes. For example, the diffraction peaks shown on the XRD pattern 3 in Figure 4a indicate that a mixture of t-Se and β-Ag_2Se was only obtained after the reaction lasted 7 d at RT. The EDX result

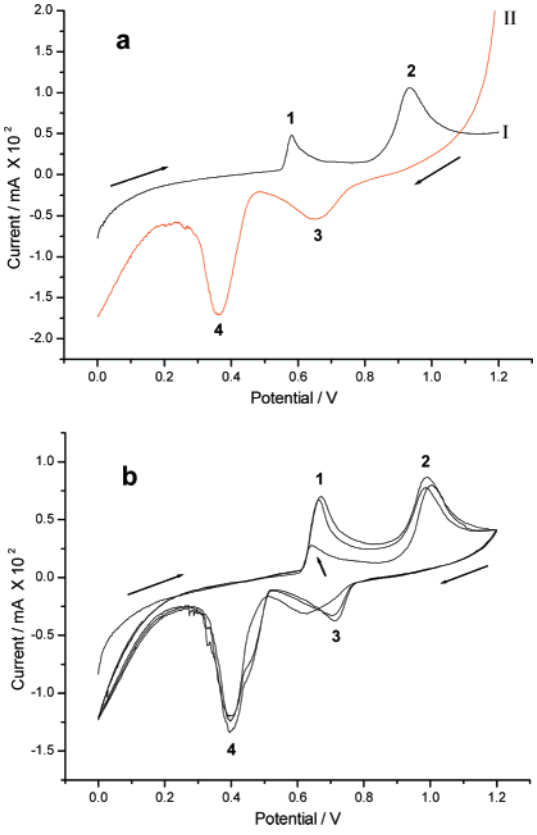

Figure 5. The voltammograms of Ag_2Se nanotubes in 0.10 mol/L KNO_3: (a) the positive-going scan voltammogram (curve I) and the negative-going scan voltammogram (curve II); and (b) three successive cyclic voltammograms.

shows that the atom ratio of the Ag and Se in this mixture is 35.91:64.09, and the SEM image (Figure 4b) shows that the morphology of this mixture is tubular. By a reaction period of 10 d at RT, the t-Se nanotubes were completely transformed to Ag_2Se nanotubes, which is made clear by the XRD pattern 4 in Figure 4a where the diffraction peaks of t-Se all disappeared. According to Su et al.'s result,[23] the slowness of this transformation process resulted from the slow diffusion of Ag^{1+} species into the crystal lattice of t-Se nanotubes, as well as the slow disproportion of Se^0 to Se^{2-} and Se^{4+} at low temperature.

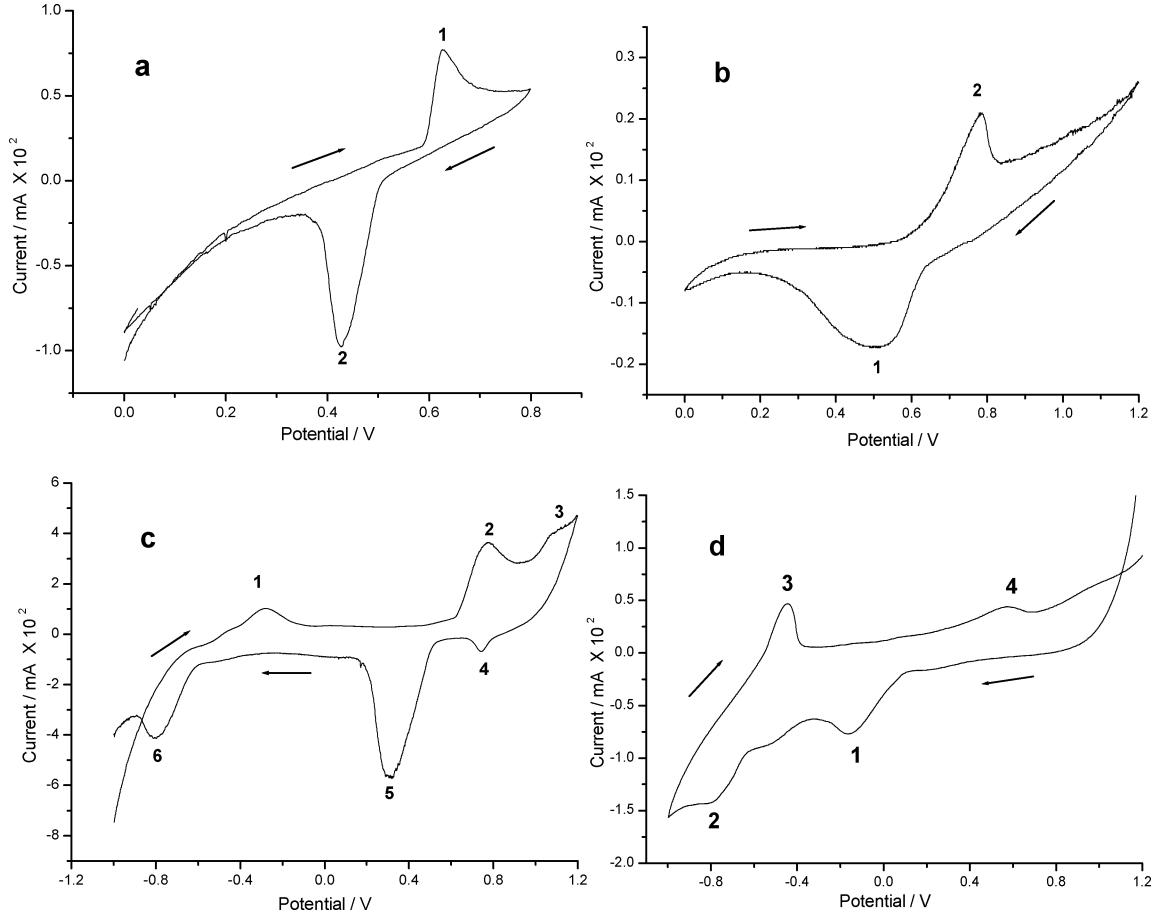

Figure 6. The cyclic voltammograms obtained: (a) in narrow scan scope for Ag_2Se nanotubes; (b) for $AgNO_3$ solution; (c) in wide scan scope for Ag_2Se nanotubes; and (d) for SeO_2 solution.

Apart from the function of the temperature, the atom ratio of the Ag and Se in the precursors plays an important role in the synthesis of Ag_2Se nanotubes. The experimental results indicate that the excessive Ag^{1+} species in the precursors could accelerate the transition from t-Se nanotubes to Ag_2Se nanotubes. As above, at RT, it took 10 d to completely transform t-Se nanotubes to Ag_2Se nanotubes with the atom ratio 3:1 of Ag and Se in the precursors. When this atom ratio was increased to 10:1 and 20:1, the Se nanotubes could be completely transformed to Ag_2Se nanotubes in 3 and 1 d at RT, respectively.

Electrochemistry. It has been reported that the electrode reaction of Ag_2Se follows a complex mechanism, due to the versatility of Se species, such as Se^0, Se^{2-}, Se^{4+}, and Se^{6+}.[24] Figure 5 shows our experimental results for the Ag_2Se nanotubes by linear scan voltammetry. From Figure 5a, it can be seen that there are two anodic peaks on curve I. Consulting the report results that the Ag_2Se could be oxidized to Se^0 and Ag^{1+} at 0.75 V (vs SCE),[25] and then the Se^0 could be oxidized to Se^{4+} at 0.98 V (vs SCE),[26] we attribute the anodic peak 1 (at 0.58 V) to the oxidation of the Ag_2Se nanotubes ($Ag_2Se \rightarrow Se^0 + 2Ag^{1+} + 2e$) and the anodic peak 2 (at 0.93 V) to the oxidation of Se^0 ($Se^0 \rightarrow Se^{4+} + 4e$). Thus, the catholic peak 3 (at 0.65 V) and catholic peak 4 (at 0.37 V) on curve II are assigned to the reduction of Se^{4+} ($Se^{4+} + 4e \rightarrow Se^0$) and the reduction of Ag^{1+} ($Ag^{1+} + e \rightarrow Ag^0$), respectively.

Figure 5b shows the successive cyclic voltammograms of the Ag_2Se nanotubes. Noticeably, peak 1 in the first cycle voltammogram (as arrowed in Figure 5b) is low and then boosted up in the second and third cyclic voltammograms. This phenomenon can be explained as that peak 1 in the first cycle originated from the oxidation of Ag_2Se nanotubes, and in subsequent cycles came from the oxidation of Ag^0 that had been produced by the reduction of Ag^{1+} (peak 4 in Figure 5b). After the first cycle, the redox peaks in cyclic voltammograms were all produced by two reversible redox couples: Se^{4+}/Se^0 and Ag^{1+}/Ag^0.

To verify the above designations, several experiments were carried out, and the results are shown in Figure 6. When the scan potential scope for Ag_2Se nanotubes was narrowed from 0−1.2 to 0−0.8 V, only two peaks appear in the cyclic voltammogram (Figure 6a). This phenomenon can be explained as that the Se^0 produced by the oxidation of Ag_2Se nanotubes had not been further oxidized in this potential scope; therefore, the oxidation peak (peak 2 in Figure 5) of Se^0 and the reduction peak (peak 3 in Figure 5) of Se^{4+} disappeared here. Obviously, two remainder peaks (Figure 6a) resulted from the oxidation of the Ag_2Se nanotubes (peak 1) and the reduction of Ag^{1+} (peak 2). If the Ag_2Se nanotubes were substituted by $AgNO_3$ solution in the preparation of CPE, two peaks were produced in the cyclic voltammogram (Figure 6b). Clearly, the cathodic peak 1 (at 0.50 V) originated from the reduction of Ag^+ and the anodic peak 2 (at 0.78 V) came from the oxidation of Ag^0, which supports the designations about peaks 4 and 1 in Figure 5b, respectively.

Figure 6c shows the cyclic voltammogram of Ag_2Se nanotubes in wide scan potential scope. Consulting the results reported,[24] the anodic peak 1 (at −0.3 V) is due to the oxidation of Se^{2-} to Se^0. Here, the Se^{2-} was produced by the reduction of Ag_2Se nanotubes ($Ag_2Se + 2e \rightarrow Se^{2-} + 2Ag^0$) on starting scan at −1.0 V, which is manifested by the large cathodic current at this potential spot. Next, the anodic peak 2 (at 0.7 V) did not result from the oxidation of Ag_2Se nanotubes but from the oxidation of Ag^0. Based on the above discussion, peaks 3−5

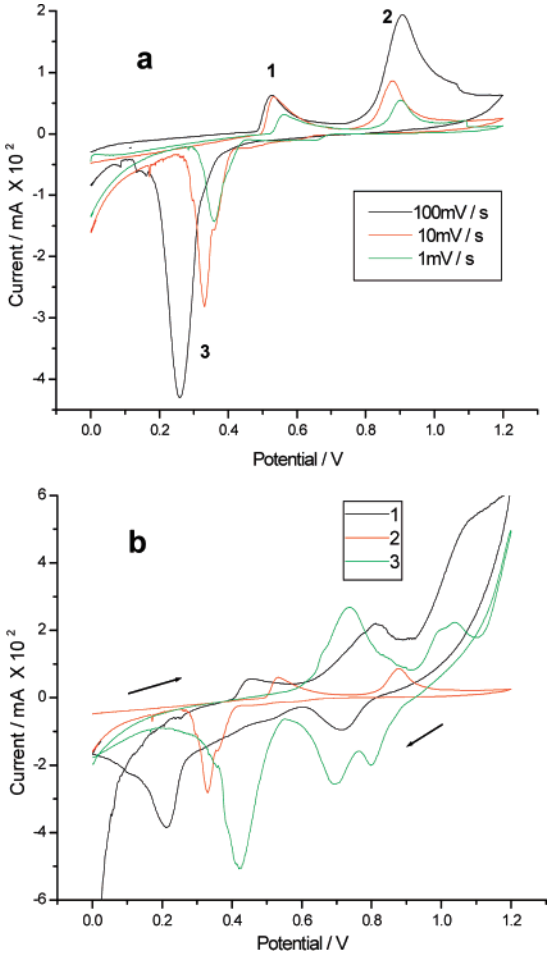

Figure 7. The cyclic voltammograms of Ag_2Se nanotubes: (a) at different scan rate in 0.10 mol/L KNO_3; and (b) in 0.10 mol/L HNO_3 (curve 1), in 0.10 mol/L KNO_3 (curve 2), and in 0.10 mol/L NaOH (curve 3).

can be designated to the oxidation of Se^0 to Se^{4+}, the reduction of Se^{4+} to Se^0, and the reduction of Ag^+ to Ag^0, respectively. Finally, the cathodic peak 6 at very low potential (−0.8 V) originated from the reduction of Se^0 to Se^{2-}.[24]

To further validate the above designations, the cyclic voltammogram of SeO_2 was determined with carbon paste electrode, and the result is shown in Figure 6d. According to Espinosa et al.'s result,[26] the cathodic peak 1 (at −0.15 V) corresponds to the reduction of SeO_2 to Se^0. This cathodic peak potential is much lower than that (at 0.7 V, peak 3 in Figure 5b) of Se^{4+} to Se^0 in the reaction system of Ag_2Se nanotubes. The phenomenon suggests that the Se^{4+} formed in the Ag_2Se reaction system, may be freely existed, and thus deoxidized more easily than SeO_2. Here, peaks 2 and 3 in Figure 6d, which were formed by the reduction of Se^0 to Se^{2-} and the oxidation of Se^{2-} to Se^0, respectively, confirm the designations for peaks 6 and 1 in Figure 6c. In addition, the weak peak 4 in Figure 6d may be due to the oxidation of little Se^0. Here, it is worth pointing out that the oxidation peak potential (at −0.4 V, peak 3 in Figure 6d) of Se^{2-} (existed as H_2Se or K_2Se) is much lower than that (at 0.6 V, peak 1 in Figure 5a or 6a) of the Ag_2Se, which suggests the high stability of Ag_2Se nanotubes.

The electrochemical behavior of the Ag_2Se nanotubes was further studied by changing the potential scan rate and the electrolyte solution acidity, respectively. From the cyclic voltammograms in Figure 7a, it can be seen that the potential scan rate affected the intensity and position of the peaks. Peak 1 that developed by the oxidation of Ag_2Se nanotubes to Se^0 and Ag^{1+} was rarely affected by the potential scan rate. This voltammetric characteristic may be the inherence of solid electroactive particles. Clearly, the intensity and position of peaks 2 and 3 that originated from Se^0 and Ag^{1+}, respectively, are nearly relevant with the potential scan rate. This relationship is the voltammetric characteristic of the hydroponic diffusibility particle, which suggests that the Ag^{1+} may exist as $Ag(H_2O)^{1+}$ and the Se^0 did not agglomerate before being oxidized to Se^{4+} in the reaction system of Ag_2Se nanotubes.

From the cyclic voltammograms in Figure 7b, it can be seen that the electroactivity of Ag_2Se nanotubes in acidic or alkaline solution is increased, as compared to that in neutral KNO_3 solution. In acidic solution, as shown on curve 1 in Figure 7b, the large cathodic current on starting scan (at ca. 0 V) may result from the reduction of Ag_2Se to Ag^0 and H_2Se. Thus, the anodic peak at 0.4 V, anodic peak at 0.8 V, and shoulder anodic peak at 1.1 V originated from the oxidation of H_2Se to Se^0, Ag^0 to Ag^{1+}, and Se^0 to Se^{4+}, respectively. As compared to the corresponding anodic peak (at 0.9 V, as shown on curve 2 in Figure 7b) in neutral solution, this shoulder anodic peak is positively shifted due to the difficulty of Se^0 oxidation in acidic solution.[21] In alkaline solution, the large anodic peak (at 0.7 V on curve 3 in Figure 7b) may result from the oxidation of Ag_2Se to Ag^{2+} (AgO) and Se^0, due to the easier oxidation for Ag^{1+} in alkaline solution. Also, the wide anodic peak at 1.0 V originated from the oxidation of Se^0 to Se^{4+} along with Se^{4+} to Se^{6+}, due to the easy oxidation for Se^0 in alkaline solution.[21] Consequently, the successive two cathodic peaks at ca. 0.75 V resulted from the reductions of Se^{6+} to Se^{4+} and Se^{4+} to Se^0. In alkaline solution, the large cathodic peak (at 0.4 V on curve 3) may originate from the reduction of Ag^{2+} (AgO) to Ag^0 but not from the reduction of Ag^{1+} (Ag_2O) to Ag^0 whose peak potential should shift negatively, as compared to that (at 0.2 V on curve 1) of Ag^{1+} to Ag^0 in acidic solution. These designations need to be further validated by another method.

Conclusion

In summary, Ag_2Se nanotubes were prepared by the template-engaged synthesis in which the trigonal Se nanotubes as-prepared were used as template reagent. The XRD pattern indicates that the Ag_2Se nanotubes possess the structure of orthorhombic phase. The ED pattern confirms that the Ag_2Se nanotubes are single crystalline. The effects of the temperature and the atom ratio of Ag and Se in the precursors on the product were studied, respectively. Besides the synthesis, the electrochemical behavior of the Ag_2Se nanotubes was examined in different conditions. The results show that the electrode reaction of Ag_2Se nanotubes is irreversible and the electroactivity of Ag_2Se nanotubes in acidic or alkaline condition is increased, as compared to that in neutral condition. Especially, the Ag_2Se nanotubes may be oxidized to Ag^{2+} and Se^{6+} in alkaline condition. The Ag_2Se nanotubes as-prepared might be useful as promising materials for the fabrication of low-temperature thermoelectric devices and as small containers for a variety of applications. The electrochemistry characteristics observed, along with the optical properties, are significant for the use of Ag_2Se nanotubes in nanoscale electronic and optoelectronic devices.

Acknowledgment. Support for this work from the National Natural Science Foundation of China (Nos. 20475001, 50532030, 20471001), the Anhui Research Project (Nos. 050440702, 2005KJ011ZD, 2006KJ007TD), and the Shanghai Research Project (No. 05JC14059) is gratefully acknowledged.

References and Notes

(1) Kobayashi, M. *Solid State Ionics* **1990**, *39*, 121.
(2) Shimojo, F.; Okazaki, H. *J. Phys. Soc. Jpn.* **1993**, *62*, 179.
(3) Lewis, K. L.; Pitt, A. M.; Wyatt-Davies, T.; Milward, J. R. *Mater. Res. Soc. Symp. Proc.* **1994**, *374*, 105.
(4) Kumashiro, Y.; Ohachi, T.; Taniguchi, I. *Solid State Ionics* **1996**, *86*−*88*, 761.
(5) Xu, R.; Husmann, A.; Rosenbaum, T. F.; Saboungi, M. L.; Enderby, J. E.; Littlewood, P. B. *Nature* **1997**, *390*, 57.
(6) Gesa, B.; Jürgen, J. *Physica B* **2001**, *308*−*310*, 1086.
(7) Das, V. D.; Karunakaran, D. *Phys. Rev. B* **1989**, *39*, 10872.
(8) Ferhat, M.; Nagao, J. *J. Appl. Phys.* **2000**, *88*, 813.
(9) Byron, G.; Wu, Y. Y.; Yin, Y. D.; Yang, P. D.; Xia, Y. N. *J. Am. Chem. Soc.* **2001**, *123*, 11500.
(10) Damodara, V.; Karunakaran, D. *J. Appl. Phys.* **1990**, *67*, 878.
(11) Okabe, T.; Ura, K. *J. Appl. Crystallogr.* **1994**, *27*, 140.
(12) Safran, G.; Geszti, O.; Radnoczi, G.; Barna, P. B. *Thin Solid Films* **1998**, *317*, 72.
(13) Pejova, B.; Najdoski, M.; Grozdanov, I.; Dey, S. K. *Mater. Lett.* **2000**, *43*, 269.
(14) Batabyal, S. K.; Basu, C.; Das, A. R.; Sanyal, G. S. *Cryst. Growth Des.* **2004**, *4*, 509.
(15) Zhan, J. H.; Yang, X. G.; Li, S. D.; Wang, D. W.; Xie, Y.; Qian, Y. T. *Int. J. Inorg. Mater.* **2001**, *3*, 47.
(16) Tan, H.; Li, S. P.; Fan, W. Y. *J. Phys. Chem. B* **2006**, *110*, 15812.
(17) Zhu, W.; Wang, W. Z.; Shi, J. L. *J. Phys. Chem. B* **2006**, *110*, 9785.
(18) Gates, B.; Mayers, B.; Wu, Y. Y.; Sun, Y. G.; Cattle, B.; Yang, P. D.; Xia, Y. N. *Adv. Funct. Mater.* **2002**, *12*, 679.
(19) Jiang, Z. Y.; Xie, Z. X.; Zhang, X. H.; Huang, R. B.; Zheng, L. S. *Chem. Phys. Lett.* **2003**, *378*, 313.
(20) Bernard Ng, C. H.; Tan, H.; Fan, W. Y. *Langmuir* **2006**, *22*, 9712.
(21) Zhang, S. Y.; Liu, Y.; Ma, X.; Chen, H. Y. *J. Phys. Chem. B* **2006**, *110*, 9041.
(22) Zhang, H.; Zuo, M.; Tan, S.; Li, G. P.; Zhang, S. Y.; Hou, J. G. *J. Phys. Chem. B* **2005**, *109*, 10653.
(23) Su, H. L.; Xie, Y.; Li, B.; Qian, Y. T. *Mater. Res. Bull.* **2000**, *35*, 465.
(24) Perdicakis, M.; Grosselin, N.; Bessikre, J. *Electrochim. Acta* **1997**, *42*, 3351.
(25) Luo, R.; Rice, N. M.; Taylor, N.; Gee, R. *Hydrometallurgy* **1997**, *45*, 221.
(26) Espinosa, A. M.; Tascon, M. L.; Vazquez, M. D.; Batanero, P. S. *Electrochim. Acta* **1992**, *37*, 1165.